Bull. Chem. Soc. Ethiop. **2024**, 38(5), 1453-1468.
DOI: https://dx.doi.org/10.4314/bcse.v38i5.20

ISSN 1011-3924
Printed in Ethiopia
Online ISSN 1726-801X

A NOVEL COMPOSITE LA-CONVERSION COATINGS FOR ENHANCED ANTI-CORROSION PERFORMANCE UNDER A HARSH AQUEOUS ENVIRONMENT

Haewon Byeon[1], M.S. Sivagama Sundari[2*], Ilango Karuppasamy[2] and R.S. Jayaram[3]

[1]Inje University, Medical Big Data Research Center, Gimhae 50834, South Korea
[2]Department of Electrical and Electronics Engineering, Amrita School of Engineering, Coimbatore, Amrita Vishwa Vidyapeetham, India
[3]Department of Mechanical Engineering, Amrita College of Engineering and Technology, Nagercoil, India

(Received March 6, 2024; Revised April 8, 2024; Accepted April 21, 2024)

ABSTRACT. The ceramic lanthanum nanoparticles with uniformly dispersed spherical nanostructures were successfully synthesized using sonication-assisted synthesis. The morphologies and phase compositions were assessed and investigated. The electrochemical impedance analysis potentio-dynamic polarisation measurements were used to calculate the corrosion protection properties of prepared ceramic lanthanum nanoparticles. The La_2O_3 nanoparticles were added as a surface coating layer to enhance the corrosion resistance of low-carbon steel. The particles' impact on coating development, morphology, and corrosion inhibition efficacy were studied. After particle integration, results show a dramatic reduction in porosity and thickness, affecting corrosion resistance. Incorporating ceramic lanthanum nanoparticles into a coating reduces porosity and increases hardness, improving corrosion resistance; the result implies the suggested technique is viable for creating functionalized coatings on low-carbon-based materials. The results also demonstrated that these methods may increase the development and protectiveness of the coating. There was a crucial nano particulate La_2O_3 level at which the conversion coatings exhibited the best protective qualities. As it increased the corrosion potential and lowered the anodic current, the composite La-conversion coatings may offer substantial corrosion protection for prolonged immersion in a 3.5% NaCl solution.

KEY WORDS: Ceramic nanoparticles, Low carbon steel, Corrosion prevention, Polarization

INTRODUCTION

One of the primary areas of focus is advancing organometallic or inorganic chemicals to facilitate the synthesis of nanoparticles. Using the novel molecule has potential benefits and presents a novel strategy for synthesizing nanomaterials, enabling control over nanocrystal characteristics such as size, shape, and dispersion [1]. The decrease of particle size to the nanoscale scale yields a range of intriguing features when contrasted to the qualities exhibited by bulk materials. Due to their vast surface area, metal oxide and hydroxide nanoparticles significantly benefit traditional materials in several applications. Within the ever-evolving field of materials science and engineering, the continuous endeavour to discover innovative materials with unique characteristics persists as an enduring endeavour [2]. The development of effective anti-corrosion coatings is one area that is of the utmost significance in this pursuit. These coatings are intended to safeguard essential infrastructure, industrial equipment, and consumer items from the persistent bombardment of corrosives. Corrosion, often known as the "silent adversary," has substantial economic and safety implications, resulting in yearly costs of billions of dollars and compromising the structural integrity of various infrastructures and equipment. In addition to its economic importance, corrosion has the potential to frustrate safety measures, resulting in severe breakdowns within essential systems, presenting environmental risks, and endangering the safety of people. To address this widespread issue, researchers persistently investigate novel

*Corresponding authors. E-mail: ms_sivagamasundari@cb.amrita.edu

methodologies for developing corrosion-resistant materials. In the present circumstances, the search for novel and efficient strategies to combat corrosion is of utmost importance [3]. Traditional processes, such as painting and coating, possess some limits, particularly when subjected to challenging conditions characterized by mechanical damage, intense temperatures, and chemical exposure. Therefore, researchers have redirected their focus towards new materials that possess intrinsic resistance to corrosion as an alternate strategy.

The lanthanum oxide (La_2O_3) is a compound that has garnered significant attention in research due to its remarkable chemical stability, elevated melting point, and capacity to generate passive oxide layers. Lanthanum is classified as a rare earth element, and its compounds, such as lanthanum oxide, play a crucial role in fabricating other rare earth elements and their alloys are of utmost importance in various advanced technological applications. The La_2O_3 has many notable benefits, which include a high melting point, exceptional chemical stability, dielectric properties, catalytic properties, optical applications, battery technology, phosphors for lighting, fuel cells, anticorrosion coatings, and being utilized as an additive in ceramics. These properties frame it as a promising contender for applications to prevent corrosion [4]. Using sonochemistry, the objective is to exploit the inherent characteristics of this technique to develop corrosion-resistant coatings that exhibit exceptional effectiveness. Nanomaterials have a high specific surface energy and surface area, high catalytic activity, a small melting point, antimicrobial characteristics, and strong photosensitivity. In recent years, nanomaterials have been extensively used in various industries, including catalysis, microelectronics packaging, metallurgy, and ceramics. Controlling the size and shape of nanoparticles being synthesized has become a significant issue because the characteristics of nanomaterials are highly dependent on their shape and size [5]. On the other hand, nanomaterials can quickly form aggregations or accumulations due to the small size of their particles. This can lead to a significant decline in the attributes of the nanomaterials. In light of this, using ultrasonic treatment is presented as a viable strategy for synthesizing dispersed nanomaterials that contain tiny particles or grains. When comparing ultrasonic treatment to other synthesis methods such as bead milling, optical tweezers, magnetic fields, and electric fields, it exhibits several advantages. These include a high frequency, effective transmissibility & directionality, concentrated energy, significant reflectivity, and convenient accessibility. In addition, ultrasonic treatment is a more accessible option and it has been extensively used in synthesizing nanomaterials and their composites. Catalytic materials, metal nanoparticles, colloidal sols, and proteins are only some of the examples of these types of materials [6].

Researchers persistently investigate novel approaches for developing corrosion-resistant materials to address this widespread issue. One such technique that has been used is the synthesis of La_2O_3 by applying the sono-chemical process. Sonochemistry has emerged as a flexible and sustainable technique for material synthesis, whereby chemical reactions are induced by using high-intensity ultrasonic vibrations. It offers several advantages and imparts unique properties to materials synthesized through this method. The utilization of this method has several benefits, including rapid reaction kinetics, precise regulation of particle dimensions, structure, and the capacity to produce materials at comparably lower temperatures which makes the sonochemistry an appealing option for creating sophisticated materials to prevent corrosion [7]. Another review comprehensively discusses the construction and application of superhydrophobic surfaces incorporating graphene. It underscores the remarkable effectiveness of graphene-based superhydrophobic coatings, specifically in showcasing exceptional anticorrosion properties. The comprehensive portrayal delves into the advantages of graphene and its derivatives in enhancing the superhydrophobicity of a wide range of metals and alloy substrates [8]. Researchers dedicated their efforts to formulating a proficient solid-state welding technique for AA8011 alloy welding. A thorough comparison was conducted between the friction stir welded specimens and the base material, assessing various factors such as microhardness, tensile strength, joint efficiency, elongation, corrosion rate, and wear rate. Subsequent to the tensile test, fractography analysis was

carried out, and scanning electron microscopy was employed to examine the surface morphology following corrosion and wear tests [9]. Some researchers concentrate on exploring the collaborative interplay between materials and coating technologies, shedding light on their joint contribution to enhancing the anticorrosive properties of superhydrophobic coatings. The analysis encompasses the impact of materials, spanning metallic, non-metallic, and hybrid classifications, each characterized by distinctive structural features and energy properties that enhance anti-corrosive performance. Moreover, the review underscores the significance of dynamic fabrication strategies, emphasizing their crucial role in achieving improved corrosion inhibition activities [10]. Researchers investigate and compare the tensile strengths of different samples comprised of aluminium alloy AA8011, both before and after experiencing corrosion. The study utilizes the Linear Radial Basis Function (LRBF) model to graphically represent and comprehend the data. It concludes that specimens subjected to a welding speed (WS) of 45 mm/min, a shoulder diameter (SD) of 21 mm, and a tool rotation speed (TRS) of 1200 rpm demonstrate the highest tensile strength among the specimens, both pre- and post-corrosion [11].

The present study aims to explore the synthesis of La_2O_3 by using sonochemistry as a unique method, focusing on its potential use in corrosion prevention. Moreover, this research extends the scope of investigation by utilizing three different acidic, basic, and neutral electrolytes (1 M KOH, 1 M HCl, and 3.5 wt.% NaCl) during the synthesis process, aiming to reveal the distinctive characteristics and performance variations of the resultant La_2O_3 coatings. Thus, the comprehensive investigation of the synthesis of La_2O_3 via sonochemistry and its application for anticorrosion purposes using three distinct electrolytes has been examined and investigated using several physicochemical techniques, with optical properties examined through ultraviolet (UV) spectroscopy and morphological analysis via scanning electron microscopy (SEM), along with EDAX and corrosion studies examined using different electrolytes and electrodes.

EXPERIMENTAL

The precursor material used in the present experiment was lanthanum(III) nitrate hexahydrate ($La(NO_3)_3.6H_2O$), whereas ammonia (NH_4OH) was used as the reducing agent for the synthesis of ceramic lanthanum oxide nanoparticles. Furthermore, the washing process comprised ethanol and distilled water as solvents, in addition to the aforementioned compounds.

Synthesis of ceramic lanthanum nanoparticles

To produce the ceramic La_2O_3 nanoparticles, 100 mL of distilled water were given 0.1 M of lanthanum nitrate to dissolve. While vigorously stirring the mixture, the stoichiometrically appropriate quantity of lanthanum nitrate solution was added gradually.

As stated earlier, the solution was stirred for 30 minutes before ammonia was added to it progressively until it reached a pH of 10. Subsequently, the solution was transferred to a probe-type sonicator operating at a frequency of 40 kHz. The sonicator was used to subject the solution to sonication for duration of one hour. The temperature of the solution reached a high of 50 ºC while it was being sonicated. After drying for 3 hours at 6 ºC in the air, the final product was finely ground. The ultrafine particles were calcined in a muffle furnace at 500 ºC for 3 hours [12], as shown in Figure 1(a).

Electrochemical measurements

The investigation evaluated the corrosion prevention properties of the synthesised ceramic La_2O_3 nanoparticles using a low-carbon steel (LCS) plate as the test substrate. The LCS metal plate was cleaned using acetone and then polished using silicon carbide grit sheets with a thickness of 1 mm. To create slurry, a mixture was prepared by combining ceramic La_2O_3 nanoparticles with N-

methyl-2-pyrrolidone and polyvinylidene fluoride in weight proportions of 80:15:5. The coating of the slime onto the LCS plate was performed using the doctor blade technique [13]. The plate that had been coated underwent a drying process lasting for 1 hour at 353 K temperature. Subsequently, it was cooled down, and corrosion experiments were conducted using electrolytic solutions that consisted of 1 M H_2SO_4, 3 M KOH, and 3.5 wt.% NaCl. The corrosion investigation used a potential window extending from -1.8 to -0.4 V at a scan frequency of 5 mVS^{-1}.

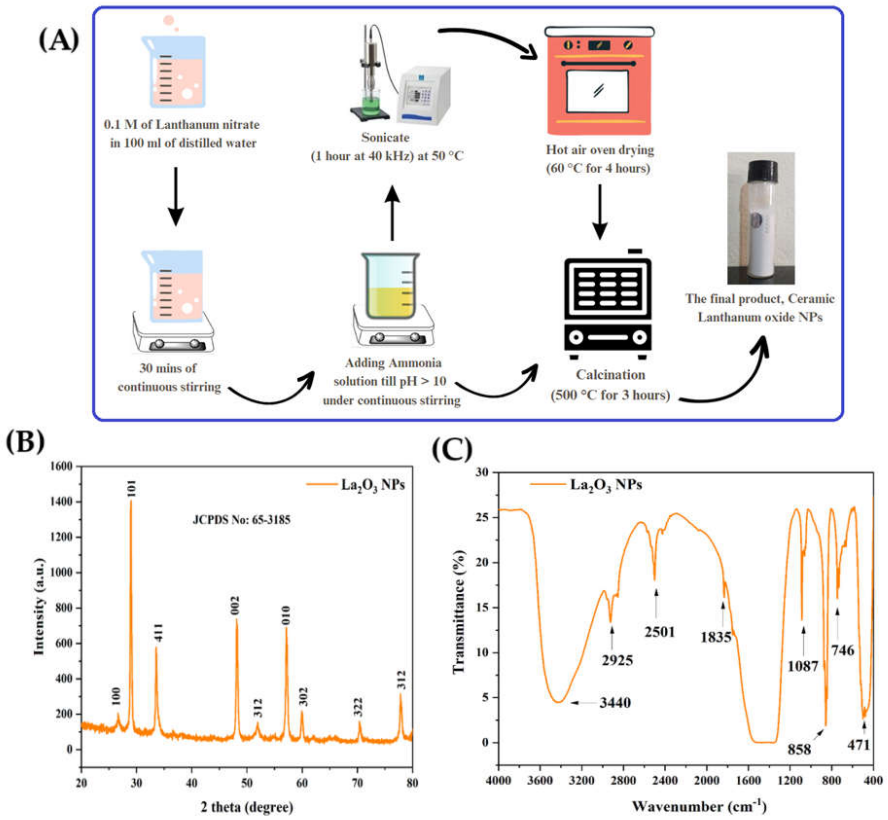

Figure 1. (a) Synthesis, (b) XRD pattern and (c) FTIR spectra of ceramic La_2O_3 nanoparticles.

Characterization

The X-ray diffractometry was used to evaluate the phase clarity and assess the prepared ceramic La_2O_3 nanoparticles structural components. The assessment was performed on XRD analysis with Cu anode. The XRD patterns were obtained at a range of 2° to 80°. The FTIR study was conducted for functional group identification of the prepared ceramic La_2O_3 nanoparticles in the vicinity of 4000 to 400 cm^{-1}, using KBr in the ratio of 200:1. To know the average particle size distribution, a particle size analyzer study was performed, at a wavelength of 633 nm using a laser beam by light scattering technique. The technique was performed several times to get the optimized data to acquire an average particle size [14]. To study the optical absorbance of ceramic La_2O_3 nanoparticles, UV-Vis spectroscopy was performed and DD water as a solvent in the electromagnetic spectral wavelength ranging from 180 to 800 nm. The bandgap of ceramic La_2O_3

nanoparticles is calculated with the results of UV-Vis spectroscopy by employing Tauc relations. Surface topology and morphological characteristics of ceramic La_2O_3 nanoparticles were considered using high resolution transmission electron microscopy at 200 kV in addition to energy dispersive X-ray spectroscopy (EDX) with elemental mapping analysis. Photoluminescence spectroscopy was used to investigate the electronic and optical properties of the synthesised ceramic La_2O_3 nanoparticles. The experimental setup for the electrochemical impedance studies (EIS) and corrosion tests included using platinum wire as the working electrode, saturated calomel electrodes as the counter electrode, and counter electrodes as the reference electrodes. The electrochemical measurements were conducted using a PGSTAT302N electrochemical workstation. The surface analysis of the pristine LCS plate and the ceramic La_2O_3 nanoparticles coated plate corrosion experiments in various electrolytes was conducted using scanning probe microscopy (SPM).

RESULTS AND DISCUSSION

The X-ray diffractometer was used to conduct a structural examination of the as-prepared and calcinated samples, as seen in Figure 1(b). The diffraction pattern indicates that all samples possess a cubic crystalline structure, as shown by the JCPDF card number 65–3185. The lattice parameters for these samples are determined to be a=b=c=4.74 Å, with the angles α=β=γ=90º. The observed correlation between increased peak intensity and the corresponding increase in reaction time provides evidence for the enhancement of crystalline size in the samples. The absence of further impurity phases in the sample suggests that the produced samples exhibit high material purity. The ceramic La_2O_3 nanoparticles under investigation exhibited distinct diffraction peaks at specific angles of 31.7º, 34.5º, 36.3º, and 56.7º, which corresponded to the (100), (002), (101), and (110) crystallographic planes, respectively. Furthermore, the prominent characteristic diffraction peaks at angles of 29.1º and 45.3º exhibited the most significant proportion of La_2O_3 compared to other phases. These peaks were correlated with the Miller indices of (321) and (440), respectively. The crystallite size of the ceramic La_2O_3 NPs was estimated using the Scherrer equations based on the X-ray diffraction data. The mean crystallite size of ceramic La_2O_3 NPs is determined to be 14.59 nm. Thus, it can be concluded that pure ceramic La_2O_3 NPs crystallite size increased with increasing sonication time and other synthesis parameters. The prepared ceramic La_2O_3 NPs are stable phase and high in purity. These ceramic nanoparticles are superiorly supportive for the anticorrosion application. The lattice parameter of the prepared ceramic La_2O_3 NPs was found to be a=b=c=4.74 Å and α=β=γ=90º, volume V = 69.21Å^{3}and the d-spacing value calculated with the following formula [11].

$$d = \frac{a}{\sqrt{h^2 + k^2 + l^2}} \quad (1)$$

The crystallite sizes, FWHM values, Miller indices and d-spacing for the prepared ceramic La_2O_3 NPs are tabulated in Table 1.

Table 1. Crystallite sizes, FWHM values, Miller indices and d-spacing for the prepared ceramic La_2O_3 nanoparticles.

Miller indies	2θ (degrees)	FWHM (degrees)	Crystal size (nm)	d-spacing (nm)
101	28.9321	0.5614	18.91	0.308
411	33.5448	0.7467	11.12	0.267
002	48.1273	0.5673	15.33	0.189
010	57.1228	0.6338	14.26	0.161
302	59.895	0.7676	11.94	0.154
322	70.4748	0.6346	15.32	0.133
312	77.7978	0.6673	15.29	0.122

The vibrational properties of the ceramic nanoparticles composed of La_2O_3 were examined using FT-IR spectroscopy which is an effective analytical technique that can potentially complement the findings obtained by XRD analysis. Figure 1(C) exhibits the synthesised samples' FT-IR spectra, covering a wave number range of 400 to 4000 cm^{-1}. It demonstrates the presence of La_2O_3 has a discernible impact on the intensity and shape of the significant absorption bands. The FT-IR spectral spectrum exhibits a distinct convergence of infrared (IR) lines, essential in forming various phases of ceramic La_2O_3 nanoparticles. The optical transparency of La_2O_3 exhibits a generally high degree, which may be attributed to the concentration of lanthanum and its potential correlation with enhanced scattering phenomena [15]. The water and hydroxyl assign a weak absorption band at 3450 to 3380 cm^{-1} O-H stretching stretches. Similarly, a comprehensive and robust bond appeared at 1500 cm^{-1} to 1400 cm^{-1} due to O-H bending vibrations of water molecules. The bands observed at 2925 cm^{-1} arise concerning C-H bonding. The band at 2501, 1835 and 1087 cm^{-1} may appear from the absorption of atmospheric CO_2 and other gas molecules. The absorption bands at 858, 746 and 471 cm^{-1} represent the metal-oxygen stretching (La-O stretch), confirming the formation of ceramic La_2O_3 nanoparticles and these findings are consistent with the results reported before [16] and reveals that the La_2O_3 had the highest intensity peaks, indicating its distinctive characteristics.

The evolving morphology of as-prepared ceramic La_2O_3 nanoparticles were investigated through SEM. Figure 2 (a and b) presents SEM pictures of the ceramic La_2O_3 nanoparticles captured at different magnifications. The ceramic nanoparticles of La_2O_3 exhibited distinct variations in their structural morphologies and revealed a uniform distribution of spherical La_2O_3 NPs. The presence of lanthanum ions promotes the process of crystal nucleation by facilitating the production of small grains. However, trapping these lanthanum grains poses a challenge to overall grain development. This could be due to stress formation during the synthesis process. The ultrasonication produces an enormous number of vibrations to the lanthanum ions. The results from the Field Emission Scanning Electron Microscopy (FESEM) analysis are consistent with the previously published data, indicating that the synthesis parameters significantly impact the behaviour of La_2O_3. These structural and morphological results from XRD and FESEM analysis show that the perfect method to produce ceramic La_2O_3 NPs is the ultrasonication process [17]. Figure 2 (c) shows the TEM figures of the synthesized ceramic La_2O_3 NPs and the morphology of the sample was determined to be spherical. The existence of well-connected, easily dispersed, and uniformly distributed particles was indicated by the formation of assembled spheres of crystalline phase development [18]. Figure 2(d) shows the EDAX spectra of the prepared ceramic La_2O_3 NPs. The inset table gives the elemental composition of ceramic La_2O_3 NPs. From the EDAX spectra, it can be concluded that the prepared ceramic nanoparticles are highly pure with no other traceable impurities.

The dynamic light scattering (DLS) analysis was executed to evaluate the average particle size distribution of the synthesized ceramic La_2O_3 NPs. The histogram of DLS analysis, specifically revealed in Figure 3(a), illustrates the distribution of particle sizes in ceramic La_2O_3 nanoparticles. The observed particle sizes vary from 9 to 80 nm, with an average size of 24.93 nm. The histogram-derived frequency distribution reveals that about 75% of the particles possess a size below 60 nm. These results agree well with the FESEM and TEM images of ceramic La_2O_3 NPs. Due to the ultrasonication process, the structural modifications in nanoparticles may be attributed to the partial disruption of intermolecular hydrophobic bonds. When the particles experience shear stress and their aggregation speed increases, there is a corresponding increase in collision occurrences. As the application of ultrasonication therapy intensifies, there is a concurrent reduction in particle size, leading to a narrower range of particle sizes. The sonication process does not impact the surface charge of particles, but it does result in the formation of a new surface and a reduction in particle size. By reducing the size of the particles, there is an increase in the unrestricted area of the material. In this specific case, the particles undergo reduction due to the exerted cavitation forces. This encompasses the disintegration of agglomerates and

aggregates [19]. Ultrasonic cavitation is a highly efficient process that disrupts the cohesion of agglomerates, aggregates, and smaller particles by disrupting the vander Waals forces that hold them together. The findings derived from XRD, FESEM, and TEM analyses indicate that the fabricated La_2O_3 exhibit stability in solution and possess a high degree of dispersibility, which renders them advantageous for potential applications in corrosion prevention.

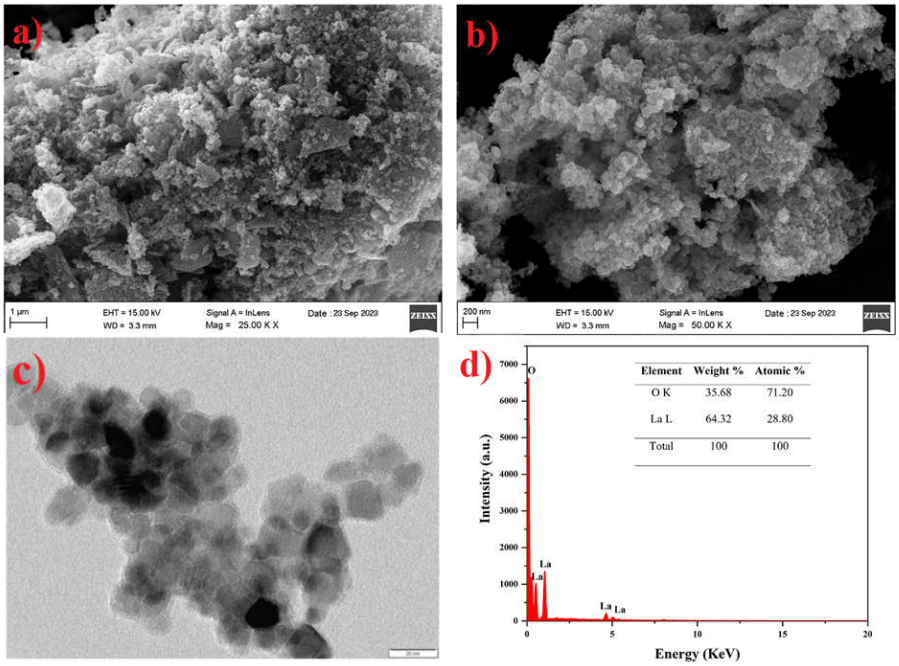

Figure 2. FESEM images (a, b), TEM image (c) and EDAX pattern (d) of Ceramic La_2O_3 nanoparticles.

The amount of light a material retains or transmits is a function of its electronic transition from the ground state to the excited state, which occurs within this electromagnetic spectrum. The prepared UV-Vis spectra of ceramic La_2O_3 NPs samples are revealed in Figure 3(b). Noticeably, the optical absorptance spectra of ceramic La_2O_3 NPs samples have appeared at only the UV range. The UV cutoff wavelength for ceramic La_2O_3 NPs samples was 197, 202, 216, and 224 nm. Based on the above findings, it is evident that the sample exhibits a minor increase in absorption and a slight decrease in transmittance after applying calculations. The observed correlation may be attributed to the decrease in particle size, as seen in SEM images. This reduction in particle size is expected to result in an enhanced surface-to-volume ratio, thereby enhancing the samples' capacity for absorption after the calcination process [20]. The UV-Vis results are in correlation with the FESEM and XRD results. The sample ceramic La_2O_3 NPs with uniformly distributed spherical morphology show a higher absorption when compared to the earlier reports. This can be accounted for the large surface area expected to be offered by the spherical morphologies. The estimated bandgap of the as-prepared and calcined materials was determined by analyzing the Tauc curve shown in Figure 3(c), obtaining a value of 5.47 eV. The high bandgap nanomaterials are highly supported for anticorrosion applications. Contact angle measurements are a notable criterion used in the examination of thin layer deposition on the surface of low carbon steel (LCS).

Moreover, the surface degradation of LCS in different electrolytes, i.e., 1 M H_2SO_4, 3 M KOH and 3.5 wt.% NaCl can be evaluated from the contact angle measurements in the presence and absence of the prepared ceramic La_2O_3 NPs coating. The phenomenon of surface deterioration in the LCS has resulted in the formation of corrosion products and an accompanying increase in surface roughness. The assessment of surface deterioration of LCS may be conducted using 1 M H_2SO_4, 3 M KOH, and 3.5 wt.% NaCl basic electrolyte for both uncoated and ceramic La_2O_3 NPs coated LCS plates. This evaluation involves measuring water contact angle values, as outlined in the Experimental section. From earlier reports on contact angle measurements of LCS, the obtained reports show better contact angle values for uncoated LCS plates. This may occur due to the proper cleaning on the surface of the LCS by applying an ultrasonication process for LCS plate surface cleaning. The contact angle data of ceramic La_2O_3 NPs coated LCS (LCS-L) show an increase in contact angle. This may be due to the thin layer of ceramic La_2O_3 NPs coating. The coating repulses the aqueous contact from the surface of LCS. Based on the results obtained, it can be assumed that applying a thin coating of ceramic La_2O_3 nanoparticles on the surface of LCS led to a reduction in surface deterioration. This may be attributed to the creation of adsorbed thin film layers, which subsequently decreased surface roughness [21]. Additionally, applying a thin layer of ceramic La_2O_3 nanoparticles on the surface of LCS enhances its hydrophobic properties, primarily attributed to the presence of hydrophobic octadecyl and oleyl tails. These factors contribute to an elevation in the contact angle. The corrosion inhibition efficiency of the thin layer of ceramic La_2O_3 NPs coating on the surface of the LCS metal plate can be evaluated using the polarization test and electrochemical impedance spectroscopy (EIS).

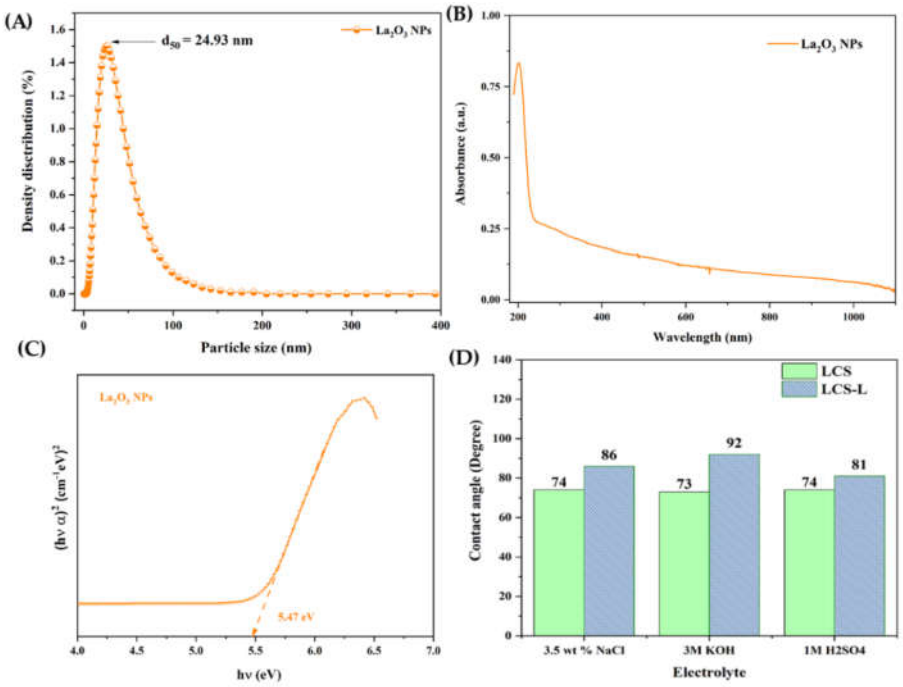

Figure 3. (a) Average particle size distribution, (b) UV-Vis absorption spectra, (c) Tauc plot bandgap energy and (d) Wettability analysis (Contact angle measurement) of Ceramic La2O3 nanoparticles.

The contact angle values of the LCS plate under various electrolytes used for electrochemical analysis are shown in Figure 3(d). The contact angle value of uncoated LCS is 74º, 73º and 74º, individually, for 1M H_2SO_4, 3 M KOH and 3.5wt. % NaCl as a testing base solution. But, the ceramic La_2O_3 NPs coating on the surface of LCS shows an increment in contact angle value, i.e., 86º, 92º, 81º under the 3 M KOH, 1 M H_2SO_4 and 3.5 wt.% NaCl electrolytes, respectively.

The electrochemical impedance spectra or Nyquist plots for 1M KOH, 1M H_2SO_4 and 3.5% NaCl solutions are revealed in Figure 4 (a), (c), and (d), respectively, for LCS plates and ceramic La_2O_3 NPs covered LCS plates. At lower frequencies, a semicircular shape was seen in the Nyquist plot diagram, indicating a potential linear relationship between this shape and the charge transfer resistance linked to the corrosion process. However, it is evident that the radius of these loops varies when comparing coated and uncoated metal surfaces across all investigated electrolytes, namely 1 M H_2SO_4, 3 M KOH, and 3.5% NaCl solutions [22]. The electrochemical impedance parameters of LCS plates derived from the Nyquist plot, ceramic La_2O_3 NPs coated LCS plates under 1 M H_2SO_4, 3 M KOH, and 3.5wt.% NaCl electrolytes are tabulated in Table 2.

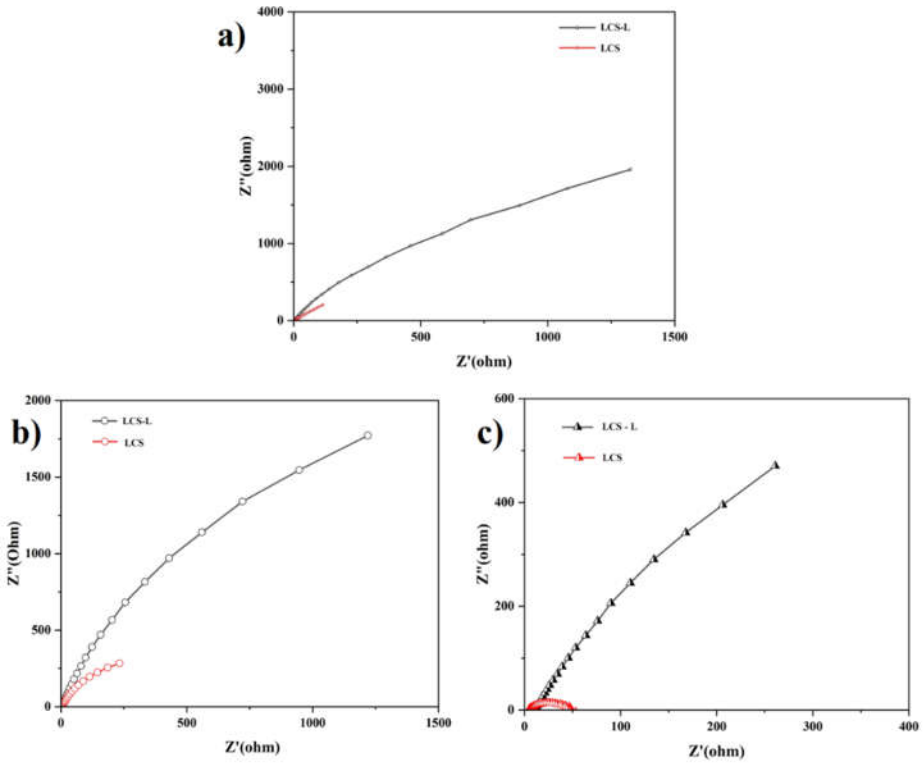

Figure 4. Nyquist plot of uncoated and ceramic La_2O_3 NPs coated LCS plate under 1 M H_2SO_4 (a), 3 M KOH (b) and 3.5 wt.% NaCl (c).

The ceramic La_2O_3 nanoparticles coated LCS plate's electrical properties exhibited greater significance than the bare LCS plate samples which indicates that the coated specimens have superior barrier capabilities in mitigating electrochemical corrosion. Remarkably, the R_{ct} values of the ceramic La_2O_3 coated on the surfaces of LCS plates exhibited greater values in 3.5% NaCl and 3 M KOH solutions compared to 1 M H_2SO_4 solutions when compared to uncoated LCS

plates. The LCS plates coated with ceramic La_2O_3 demonstrate significantly higher R_{ct} values, highlighting enhanced corrosion resistance compared to the surfaces of uncoated LCS plates. The electrochemical impedance spectra obtained from the samples using three distinct electrolytes provide evidence that the ceramic La_2O_3 nanoparticles offer substantial resistance against electrochemical corrosion. To clarify, the observed inductive response at low frequency is likely attributed to the adsorption of corrosion products on the surface of the electrode. It is important to note that all values were derived from the high capacitive loops. This phenomenon is evident from the observed rise in R_{ct} values, accompanied by a concurrent decline in the values of C_{dl}, as shown in Table 2. The augmentation of the double-layer thickness led to a drop in the double-layer capacitance (C_{dl}), which in turn caused a reduction in the dielectric constant which are attributed to the displacement of adsorbed water molecules and the adsorption of extract (organic matter) onto the surface of the mild steel.

Table 2. Electrochemical impedance parameters of uncoated and ceramic La_2O_3 NPs coated LCS plate under 1 M H_2SO_4, 3 M KOH and 3.5 wt.% NaCl.

Electrolyte	Substrate	CPE.YO	R_p.R	R_s.R	CPE.N
1 M H_2SO_4	LCS	0.00018765 F	8481.5 Ω	-7.6897 Ω	0.99633
	LCS-L	0.0012079 F	1317.6 Ω	3.8355 Ω	0.9957
3 M KOH	LCS	0.00021495 F	5885.9 Ω	2.0483 Ω	0.99734
	LCS-L	0.0018093 F	879.66 Ω	5.1879 Ω	0.99717
3.5wt. % NaCl	LCS	0.00034233 F	2455.6 Ω	11.166 Ω	0.99688
	LCS-L	0.001357 F	52.587 Ω	4.2157 Ω	0.99438

Figure 5 shows the Bode modulus and phase angle plot obtained on the uncoated LCS and ceramic La_2O_3 NPs coated LCS. The results show that the impedance values were higher for LCS plates coated ceramic La_2O_3 NPs than uncoated LCS plates in all electrolytes. As previously documented, the observed results may be attributed to the enhanced barrier characteristics and corrosion prevention capabilities. The ceramic La_2O_3 NPs coating on the LCS surface improved the corrosion protection due to increased film thickness or covering of the surface porosity. The phase angle plot is characterized by an individual time constant. A more comprehensive analysis of the electrochemical impedance spectroscopy (EIS) outcomes may be achieved by the use of numerical fitting techniques, using the equivalent circuit shown in the study which consists of an electrolyte resistance denoted as R and a coating capacitance represented as CP. Figure 6 (a, b, and c) show the potentiodynamic polarization curves, also known as Tafel plots, for LCS plates and ceramic La_2O_3 NPs coated LCS plates immersed in 1 M H_2SO_4, 3 M KOH, and 3.5% NaCl electrolytic solutions, respectively. The electrochemical corrosion parameters, namely corrosion potential (E_{corr}), corrosion rate (CR), corrosion current (I_{corr}), and polarisation resistance (R_{pol}), were determined using the Tafel plot method. These values are provided in Table 3.

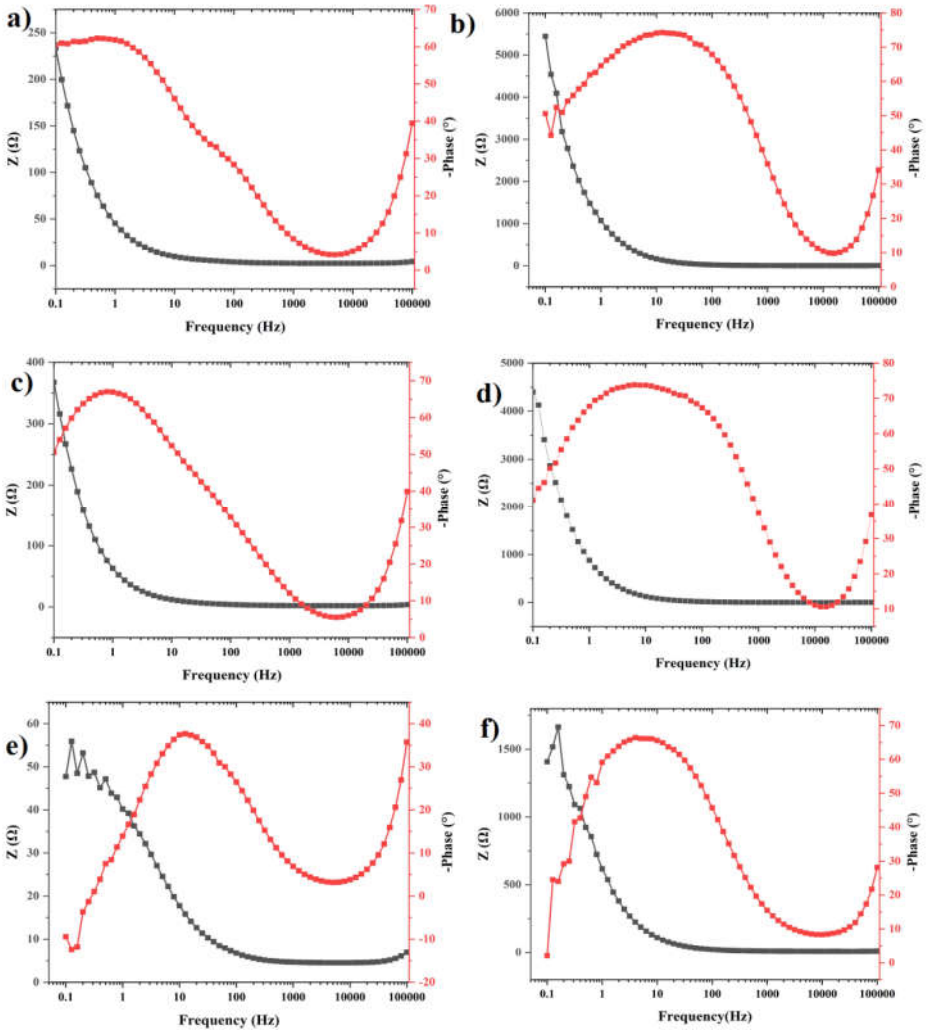

Figure 5. Bode plot of uncoated and ceramic La_2O_3 NPs coated LCS plate under 1 M H_2SO_4 (a and b), 3 M KOH (c and d) and 3.5 wt.% NaCl (e and f), respectively.

This study examines the electrochemical corrosion inhibition properties of LCS plates coated with ceramic La_2O_3 nanoparticles. The corrosion inhibition behaviours are analyzed for each electrolyte individually to facilitate interpretation and analysis. In a 1 M H_2SO_4 electrolyte medium, the corrosion potential (E_{corr}) of LCS plates coated with ceramic La_2O_3 nanoparticles was greater than that of the LCS plates without any coating. The corrosion potential (E_{corr}) of zinc (0.372 V) plates is shifted to -1.008 V as a result of the addition of a thin layer coating of ceramic lanthanum oxide nanoparticles. This decreases the ceramic La_2O_3 NPs coated LCS plates' corrosion current compared to uncoated ones. The application of a ceramic coating composed of La_2O_3 nanoparticles has been shown to have a considerable effect on the corrosion rate. The

manifestation of this effect is evident through the reduction of the corrosion current (I_{corr}) at a particular corrosion rate. In comparison to uncoated LCS plates, those coated with ceramic La_2O_3 showed a markedly increased corrosion rate, approximately 160.7 mm per year. The polarization resistance of uncoated LCS (4.018 Ω) is notably lower than the values observed for ceramic La_2O_3 nanoparticles-coated LCS plates, which registered 16.80Ω in a medium containing 1 M H_2SO_4 electrolyte. Based on the findings acquired, it can be surmised that applying a ceramic coating composed of La_2O_3 nanoparticles may serve as a viable strategy for mitigating the corrosion rate in solid acidic environments such as H_2SO_4 and HCl. The inhibitory efficiencies of the ceramic La_2O_3 nanoparticles covering were determined to be 85.77%, as shown in Table 3. The Tafel polarization curves of LCS plates ceramic La_2O_3 NPs coated LCS plates under 3 M KOH are shown in Figure 6(b). Furthermore, in 3 M KOH medium, the corrosion potential of LCS plates ceramic La_2O_3 NPs coated LCS plates was roughly 1.033 V and 1.447 V, respectively. The potential corrosion values of coated plates exhibited a substantial rise as compared to those of pure LCS plates. The corrosion rate of the uncoated low carbon steel (LCS) plate in a 3 M potassium hydroxide (KOH) electrolytic solution was very high, measuring 117.37 mm/year. Moreover, the polarization resistance exhibited a relatively high value, measuring at 4.720 Ω. In contrast, it was observed that the corrosion rate of the coated plates was relatively low, measuring 5.72 mm/year and 65.706 Ω, respectively, for the surfaces of ceramic La_2O_3 nanoparticles-coated LCS plates. These findings underscore the significance of applying a thin layer of ceramic La_2O_3 nanoparticles to the LCS surface for achieving a reduced corrosion rate and enhanced electrochemical corrosion resistance.

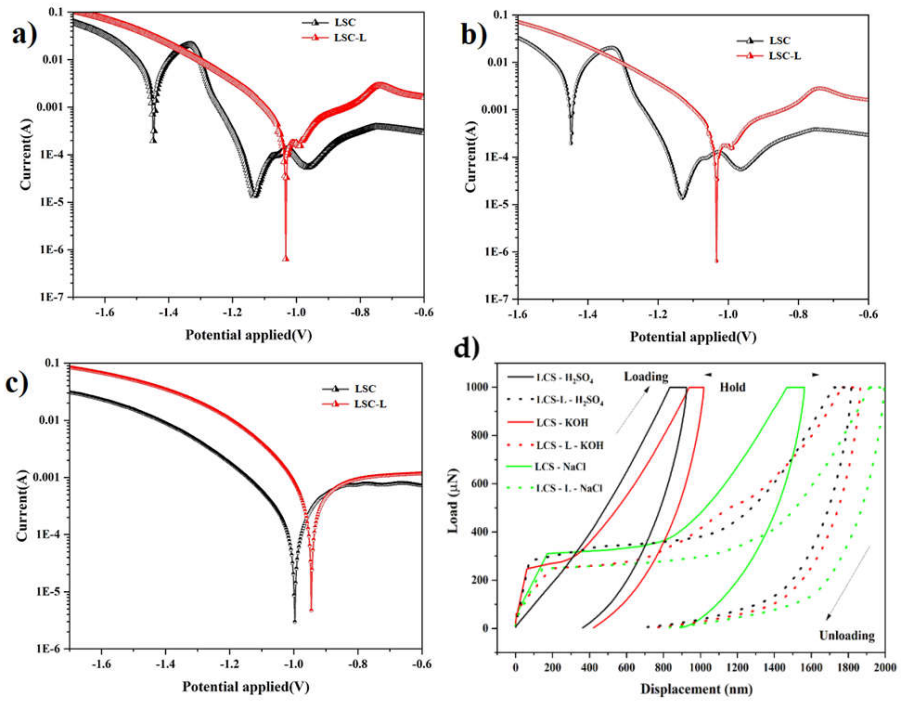

Figure 6. Tafel plot of uncoated and Ceramic La_2O_3 NPs coated LCS plate under 1 M H_2SO_4 (a), 3 M KOH (b) and 3.5 wt.% NaCl (c), Nanointendation curves of uncoated and Ceramic La_2O_3 NPs coated LCS plate under 1 M H_2SO_4, 3 M KOH and 3.5 wt.% NaCl (d).

Table 3 illustrates a notable improvement of 95.12% in corrosion prevention characteristics for the ceramic La_2O_3 nanoparticles-coated plates compared to the uncoated LCS surfaces. Conducting potentiodynamic polarization experiments on LCS (low carbon steel) and LCS plates coated with ceramic La_2O_3 NPs immersed in a 3.5% NaCl electrolytic solution revealed an anodic polarization effect on the metal plates, as illustrated in Figure 6(c). Compared to their uncoated counterparts, the coated LCS metal plates exhibited a notable capability to effectively inhibit corrosion on the metal surfaces. The corrosion potentials (E_{corr}) of LCS plates increased when coated with ceramic La_2O_3 nanoparticles (NPs) compared to uncoated LCS plates. The outcomes indicate a decrease in the corrosion rate of the coated LCS metal plates (2.40 mm/year) when contrasted with pure Zn metal plates (4.68 mm/year). An evident improvement in polarization resistance is noted for the ceramic La_2O_3 nanoparticles-coated LCS plate compared to the uncoated LCS samples. This improvement is likely associated with the reduction of La^{2+} ions.

Table 3. Parameters of potentio dynamic polarization curves (Tafel plot) of uncoated and Ceramic La_2O_3 NPs coated LCS plate under 1 M H_2SO_4, 3 M KOH and 3.5 wt.% NaCl.

Electrolyte	Substrate	E_{corr} (V)	I_{corr} (A)	Polarization resistance (Ω)	Corrosion rate (mm/year)	Efficiency (%)
1 M H_2SO_4	LCS	-0.372	$1.383x10^{-2}$	4.018	160.7	
	LCS-L	-1.008	$0.196x10^{-2}$	16.80	22.86	85.77
3 M KOH	LCS	-1.033	$1.01x10^{2}$	4.720	117.37	
	LCS-L	-1.447	$0.049x10^{2}$	65.706	5.72	95.12
3.5wt. % NaCl	LCS	-0.997	$0.403x10^{-3}$	84.03	4.68	
	LCS-L	-0.945	$0.207 x10^{-3}$	213.26	2.40	48.71

The application of a thin layer of ceramic La_2O_3 nanoparticles on the LCS surface resulted in a diminished corrosion rate and enhanced electrochemical corrosion resistance, aligning with findings from previous research. Based on the results obtained from the Tafel plot, it was shown that the ceramic La_2O_3 NPs covered LCS plate exhibited a 48.71% increase in corrosion resistance compared to the uncoated LCS metal surfaces. The findings suggest that applying a ceramic coating composed of La_2O_3 nanoparticles is crucial in forming a durable and robust protective barrier on the material's surface. This coating can potentially enhance the susceptible material's corrosion resistance. Table 4 presents a comparative analysis of the corrosion-inhibiting properties of various metal oxide nanoparticles, together with the corresponding observed results. It may be inferred that using ceramic La_2O_3 nanoparticles has shown to be advantageous in augmenting the corrosion resistance of low-carbon steel plate surfaces when exposed to an aqueous solution.

Table 4. Comparison of nanomaterial coatings on metal surfaces.

Inhibitor	Substrate	Electrolyte	Corrosion resistance efficiency (%)
ZnO	MS	3.5 % NaCl	50.11
CuO	MS	3.5 % NaCl	52.56
Mn_2O_3	MS	1 M HCl	71.53
CdS	Zn	1 M HCl	69.18
ZnS	MS	1 M HCl	72.20
NiO-Zn	MS	3.5 % NaCl	48.5
Ni-Zn-Epoxy	Steel	3.5 % NaCl	74.2
ZrO_2	316L SS	1 M H_2SO_4	67.5
La_2O_3	Low carbon steel	1 M H_2SO_4	85.77
		3 M KOH	95.12
		3.5 % NaCl	48.71

After conducting the electrochemical investigation on the LCS plates with various electrolyte solutions, a nano-indenter was utilized to determine the indentation hardness and the modulus for both the uncoated and ceramic La_2O_3-coated LCS plates. The load control method was utilized to measure the qualities of coatings utilizing a Berkovich-type indenter. The test was carried out in the order of loading, holding, and unloading, respectively. Plates were loaded until the maximum load of 1000 mN was attained to get the data shown in Figure 6(d) which depicts the plates' mean load vs. depth curves. The ceramic La_2O_3 NPs coating applied to the surface of the LCS plates caused a change in the curves toward more significant displacement values. The measured nanoindentation parameters of the uncoated and ceramic La_2O_3 NPs coated LCS plates includes displacement (nm), hardness (GPa), contact depth (nm), contact stiffness in micronewtons per nanometer, and roughness (nm). The formulation with ceramic La_2O_3 NPs coated LCS plates under KOH and NaCl electrolyte recorded the highest depth before and after the holding period. On the other hand, the uncoated plate under the NaCl electrolyte had the lowest recorded depth before and after the holding period of 30 seconds. It suggests that the ceramic coating applied to the LCS plate's surface lowered the load-bearing behaviour of the coatings. Under the influence of the KOH electrolyte, the uncoated LCS plate reached a depth of 1696.5 nm when subjected to the maximum load. The reduced stiffness caused by the ceramic La_2O_3 NPs coating on the LCS plate surface could cause a depth penetration change or decreased indentation resistance. The values of the uncoated LCS plates for 1 M H_2SO_4, 3 M KOH, and 3.5% NaCl electrolytes are 59.04 GPa, 14.13 GPa, and 74.46 GPa, respectively. Surprisingly, the electrochemical investigation reveals that the coated plates' hardness values have dropped due to their interaction with aggressive electrolytes. This demonstrates the uniformity and stability of the ceramic La_2O_3 Nanoparticles coating on the LCS plate's surface despite the surface coating not peeling off.

CONCLUSION

In the present work, ceramic La_2O_3 nanoparticles were used as an interfacial layer on the surfaces of low-carbon steel. The corrosion inhibitor characteristics of low-carbon steel were enhanced by applying a ceramic coating of La_2O_3 nanoparticles, as demonstrated by potentio dynamic polarization and EIS experiments. The EIS, contact angle and wettability investigations have additionally demonstrated that the incorporation of nanoparticles enhances the corrosion resistance of the interface of low-carbon steel. This improvement can be ascribed to the preferential movement of ceramic La_2O_3 NPs to the metal surface during the coating process, facilitated by a notable affinity between the nanoparticles and the low-carbon steel surface. It was also found that the ceramic La_2O_3 NPs significantly enhance the mechanical properties and increase the surface wettability under various aqueous electrolytes. This observation demonstrates the ability of ceramic La_2O_3 nanoparticles to enhance the corrosion resistance capabilities of low-carbon steels in aqueous conditions.

FUNDING

This research was supported by Basic Science Research Program through the National Research Foundation of Korea (NRF) funded by the Ministry of Education (NRF- RS-2023-00237287, NRF-2021S1A5A8062526) and local government-university cooperation-based regional innovation projects (2021RIS-003).

REFERENCES

1. Balabanov, S.; Filofeev, S.; Ivanov, M.; Kaigorodov, A.; Kuznetsov, D.; Hu, D.J.; Li, J.; Palashov, O.; Permin, D.; Rostokina, E. Fabrication and characterizations of holmium oxide based magneto-optical ceramics. *Opt. Mater.* **2020**, 101, 109741.

2. Díaz-Ballote, L.; Rejón, V.; Maldonado, L.; Alpuche-Avilés, M.A.; Vega-Lizama, E.T. Effect of dispersed oxide of cerium, lanthanum and thorium on the corrosion behaviour of tungsten in 3.5 Wt-% NaCl solution. *Corros. Eng. Sci. Technol.* **2023**, 58, 423-430.
3. Cheng, X.; He, Y.; Song, R.; Li, H.; Liu, B.; Zhou, H.; Yan, L. Study of mechanical character and corrosion properties of La_2O_3 nanoparticle reinforced Ni-W composite coatings. *Colloids Surf. A Physicochem. Eng. Asp.* **2022**, 652, 129799.
4. Omodara, L.; Pitkäaho, S.; Turpeinen, E.-M.; Saavalainen, P.; Oravisjärvi, K.; Keiski, R.L. Recycling and substitution of light rare earth elements, cerium, lanthanum, neodymium, and praseodymium from end-of-life applications - A review. *J. Clean. Prod.* **2019**, 236, 117573.
5. Smail, R.A.; Fadhil, F.A.; Rashed, H.H. Novel route to prepare lanthanum oxide nanoparticles for optoelectronic devices. *Int. J. Mod. Phys. B* **2020**, 34, 2050134.
6. Faznny, M.F.; Halimah, M.K.; Eevon, C.; Latif, A.A.; Muhammad, F.D.; Asyikin, A.S.; Nazrin, S.N.; Zaitizila, I. Comprehensive study on the nonlinear optical properties of lanthanum nanoparticles and lanthanum oxide doped zinc borotellurite glasses. *Opt. Laser Technol.* **2020**, 127, 106161.
7. Zhang, L.; Liu, Y.; Wang, Y.; Li, X.; Wang, Y. Investigation of phosphate removal mechanisms by a lanthanum hydroxide adsorbent using P-XRD, FTIR and XPS. *Appl. Surf. Sci.* **2021**, 557, 149838.
8. Jishnu, A.; Jitha, S.J.; Appukuttan, S.; Sethulekshmi, A.S.; Gopika, V. Superhydrophobic graphene-based materials with self-cleaning and anticorrosion performance: An appraisal of neoteric advancement and future perspectives. *Colloids Surf. A: Physicochem. Eng. Asp.* **2020**, 606, 125395.
9. Vaira, V.R.; Kumar, A.; Srirangarajalu, N.; Padmanaban, R. Investigations on the mechanical, corrosion, and tribological behavior of friction stir welded aluminum alloy AA8011. *Tran. Marit. Sci.* **2021**, 10, 20-41.
10. Krishnan, A.; Krishnan, A.V.; Ajith, A.; Shibli, S. Influence of materials and fabrication strategies in tailoring the anticorrosive property of superhydrophobic coatings. *Surf. Interf.* **2021**, 25, 101238.
11. Nischay, S.S.; Kamalesh, B.J.; Abiram, A.; Vignesh, R.V.; Padmanaban, R. Effect of corrosion on the tensile behavior of friction stir welded aluminum alloy AA 8011. *AIP Conf. Proc.* **2023**, 2492, 040021.
12. Yang, G.; Lin, W.; Lai, H.; Tong, J.; Lei, J.; Yuan, M.; Zhang, Y.; Cui, C. Understanding the relationship between particle size and ultrasonic treatment during the synthesis of metal nanoparticles. *Ultrason. Sonochem.* **2021**, 73, 105497.
13. Taghavizadeh, M.E.; Nourbakhsh, F.; Mashreghi, M.; Mousavi, S.H. Ultrasound-based synthesis of $ZnO{\cdot}Ag_2O_3$ nanocomposite: characterization and evaluation of its antimicrobial and anticancer properties. *Res. Chem. Intermed.* **2021**, 47, 1285-1296.
14. Khorasanizadeh, M.H.; Monsef, R.; Amiri, O.; Amiri, M.; Salavati-Niasari, M. Sonochemical-assisted route for synthesis of spherical shaped holmium vanadate nanocatalyst for polluted waste water treatment. *Ultrason. Sonochem.* **2019**, 58, 104686.
15. Hassen, M.M.; Ibrahim, I.M.; Abdullah, O.G.; Suhail, M.H. Improving photodetector performance of pani nanofiber by adding rare-earth La_2O_3 nanoparticles. *Appl. Phys. A: Mater. Sci. Process.* **2023**, 129, 135.
16. Li, Y.; Sun, K.; Cheng, P.; Li, J.; Liu, D.; He, D. The synergy of La_2O_3 nanoparticles and graphene for advanced Li-S batteries. *ChemistrySelect.* **2022**, 7, 36.
17. Zhang, W.; Chen, Z.; Wang, F.; Chen, X.; Mao, H. Comprehensive effects of La/B ratio and CaO additive on the efficiency of lanthanum borate glass–ceramics as sintering aids for LTCC application. *J. Mater. Sci.: Mater. Electron.* **2021**, 32, 24369-24380.
18. Garu, P.; Bag, S.P.; Pan, T.-M. High-performance solution-processed $La_2Ti_2O_7$ sensing film for a capacitive electrolyte–insulator–semiconductor pH Sensor. *IEEE Electron Device Lett.* **2021**, 42, 414-417.

19. Yao, S.; Wang, Y.; Liang, Y.; Yu, H.; Majeed, A.; Shen, X.; Li, T.; Qin, S. Modified polysulfides conversion catalysis and confinement by employing La_2O_3 nanorods in high performance lithium-sulfur batteries. *Ceram. Int.* **2021**, 47, 27012-27021.
20. Wu, L.; Zhou, Z.; Xiao, Y.; Xu, Z.; Li, X. Hydrogen evolution reaction activity and stability of sintered porous Ni-Cu-Ti-La_2O_3 cathodes in a wide pH range. *Int. J. Hydrogen Energy* **2022**, 47, 11101-11115.
21. Zhou, Q.; Zhang, L.; Wang, X. Bimetallic ZIFs derived 3D acetylene black loading La_2O_3/Co bifunctional ORR/OER catalysts. *Appl. Surf. Sci.* **2023**, 610, 155551.
22. Zheng, R.; Li, N. Mechanical properties and electrical conductivity of nano-La_2O_3 reinforced copper matrix composites fabricated by spark plasma sintering. *Mater. Res. Express* **2019**, 6, 106527.